Chapter 16
The Use of Multicomponent Solute Transport Models in Environmental Analyses

Jiří Šimůnek, Diederik Jacques, Tiago B. Ramos, and Bertrand Leterme

Abstract This chapter provides a brief overview of multicomponent solute transport models, which simulate the subsurface transport of multiple ions that may mutually interact, can create various complex species, can compete with each other for sorption sites, and/or can precipitate or dissolve. These models are broadly divided into two major groups, those with specific chemistry and general models, and typical examples of these models are given. More detail is provided for the UnsatChem and HPx modules of HYDRUS. The applicability of the UnsatChem module to simulate the multicomponent transport of major ions is demonstrated using the data from a field experiment involving irrigation with waters of different quality, carried out in Portugal. The second example illustrates the use of HP1 to simulate the fate of mercury in a contaminated soil. Finally, the third example demonstrates the versatility of HP2 to simulate the release and migration of uranium from a simplified uranium mill tailings pile toward a river. Using these three examples, it is demonstrated that in spite of the considerable demand on input data, the multicomponent solute transport models can be effective and versatile tools for evaluating complex agricultural and environmental problems.

J. Šimůnek (✉)
Department of Environmental Sciences, University of California, Riverside, CA 92521, USA
e-mail: Jiri.Simunek@ucr.edu

D. Jacques • B. Leterme
Institute for Environment, Health and Safety, Belgian Nuclear Research Centre (SCK•CEN), Boeretang 200, Mol 2400, Belgium
e-mail: djacques@sckcen.be

T.B. Ramos
CEER-Biosystems Engineering, Institute of Agronomy, Technical University of Lisbon, Tapada da Ajuda, 1349-017 Lisbon, Portugal
e-mail: tiago_ramos@netcabo.pt

W.G. Teixeira et al. (eds.), *Application of Soil Physics in Environmental Analyses: Measuring, Modelling and Data Integration*, Progress in Soil Science,
DOI 10.1007/978-3-319-06013-2_16,

Keywords Variably-saturated • Water flow • Soil • Solute transport • Multicomponent models • Hydrus • HP1 • UnsatChem • Uranium transport • Salinity • SAR • Tailings pile

16.1 Introduction

In Chap. 15 of this volume, van Genuchten et al. provided a detailed description of various approaches to modeling water flow and solute transport in soils and in unsaturated porous media in general. The focus of that chapter was on modeling the transport of only one chemical species while assuming that the behavior of this solute is independent of that of other species that may be present in the soil solution. The interaction of this species with the environment (soil) is usually described assuming linear reversible sorption (the K_d approach) and zero- or first-order reactions (production and/or decay). The advantage of this approach is that a large number of analytical solutions exist for one-, two-, and three-dimensional solute transport problems with different types of boundary conditions and steady-state water flow conditions (e.g., van Genuchten 1981; Yeh 1981; Toride et al. 1993; Leij and Bradford 1994; Šimůnek et al. 1999). These analytical models are useful for a variety of applications, such as for "providing initial or approximate analyses of alternative pollution scenarios, conducting sensitivity analyses to investigate the effects of various parameters or processes on contaminant transport, extrapolating results over large times and spatial scales where numerical solutions become impractical, serving as screening models, estimating transport parameters from laboratory or well-defined field experiments, providing benchmark solutions for more complex transport processes that cannot be solved analytically, and for validating more comprehensive numerical solutions of the governing transport equations" (van Genuchten et al. 2012).

A large number of numerical models (e.g., Šimůnek 2005; Šimůnek et al. 2008; van Genuchten et al. 2014) exists for more complex solute transport situations, such as those involving one- or multi-dimensional transient water flow, heterogeneous systems, or nonequilibrium solute transport with nonlinear reactions, for which analytical solutions are generally not available and/or cannot be derived. However, even such models represent a great simplification of real solute transport problems, since these models usually consider the transport of a single solute species, while the soil solution is always a mixture of many ions. These ions may mutually interact, can create various complex species, can compete with each other for sorption sites, and/or can precipitate or dissolve, depending on actual conditions in the soil profile (e.g., Šimůnek and Valocchi 2002; Šimůnek and van Genuchten 2006; Seaman et al. 2012). The transport codes accounting for these more complex reactions, usually called the hydrogeobiochemical transport models, offer the possibility to include processes such as aqueous complexation, cation and anion exchange, surface complexation, and/or equilibrium or kinetic precipitation/dissolution of pure solid phases or solid-solutions. In addition, they may also

consider complex parallel and/or sequential geochemical and/or microbiological kinetic networks, including soil carbon cycles, which may involve more advanced kinetic rate equations than simple zero-order or first-order reactions (e.g., Regnier et al. 2005; Thullner et al. 2005; Centler et al. 2010; Langergraber and Šimůnek 2012; Jacques et al. 2013). There are many important agricultural and environmental problems that require models capable of analyzing transport and reactions of multiple chemical species involved in such mutual interactions. In this chapter, we briefly review multicomponent solute transport models, give few typical examples (e.g., BioGeoChem, MIN3P, CrunchFlow, UnsatChem, HP1/2/3), and show a few examples of their use in agricultural (i.e., modeling of soil salinity and the fate of mercury in contaminated soil using HP1) and environmental (i.e., leaching of uranium from U tailings pile) applications.

16.2 HydroGeoBioChemical Transport Models

Reviews of the development over the last two decades of hydrogeochemical transport models involving reactive multiple components are given by Mangold and Chin-Fu Tsang (1991), Lichtner (1996), Steefel and MacQuarrie (1996), Šimůnek and Valocchi (2002), Bell and Binning (2004), Steefel et al. (2005), Seaman et al. (2012), and Šimůnek et al. (2013). Most coupled reactive transport codes were developed for steady-state flow conditions for one, two, or three dimensions, while the flow field (water contents and water fluxes) has to be specified at the input or calculated outside of the reactive transport code using other flow and transport numerical models and imported (Parkhurst and Appelo 1999; Steefel 2009; Parkhurst et al. 2004). Several multicomponent transport models have been published recently that also consider variably-saturated flow (Zyvoloski et al. 1997; Mayer et al. 2002; Jacques et al. 2006, 2008a; Šimůnek et al. 2013).

16.2.1 Models with Specific Chemistry

Geochemical models can be broadly divided into two major groups: those with specific chemistry and general models (Šimůnek and Valocchi 2002). Models with specific chemistry are usually constrained to very specific applications since they are restricted to certain prescribed chemical systems. They are, however, much easier to use since the chemical system is already predefined by model developers and can be more computationally efficient than general models because the numerics can be optimized for this particular chemical system. Typical examples of models with specified chemistry are those simulating the transport of major ions, such as LEACHM (Hutson and Wagenet 1992) and UnsatChem (Šimůnek and Suarez 1994, 1997), and various reclamation models (Šimůnek and Valocchi 2002).

These models typically consider the transport of major ions and their mutual reactions such as complexation, cation exchange, and precipitation/dissolution. The UnsatChem model, as an add-on module to HYDRUS-1D and HYDRUS (2D/3D) (Šimůnek et al. 2008), and its application to a field study will be discussed below.

Another group of models with specified chemistry are those simulating carbon and nitrogen cycles. Some examples are CENTURY (Parton et al. 1987), LEACHM (Hutson and Wagenet 1992), RZWQM (Ahuja and Hebson 1992), COUP (Jansson and Karlberg 2001), and the Wetland module of HYDRUS (2D/3D) (Langergraber and Šimůnek 2005, 2012). These models typically distribute organic matter, carbon, and organic and mineral nitrogen over multiple computational pools, while allowing organic matter to be decomposed by multiple microbial biomass populations. They can account for most of the major reaction pathways, such as inter-pool transfer of carbon and nitrogen, nitrification (ammonium to nitrate-N), denitrification (leading to the production of N_2 and N_2O), volatilization losses of ammonia (NH_3), and microbial biomass growth and death (e.g., Yuan et al. 2011).

16.2.2 General Models

Models with generalized chemistry, on the other hand, provide users with much more flexibility in designing particular chemical systems, thus permitting a much broader range of applications. Users can then either select species and reactions from large geochemical databases or are able to define their own species with particular chemical properties and reactions. However, general models require much better understanding of the chemical system involved from their users, since they themselves are responsible for correctly defining it.

As discussed above, most codes with general geochemistry are limited to solute transport and biogeochemical reactions, while water flow paths must be calculated outside of the reactive transport code. Typical examples are PHREEQC (Parkhurst and Appelo 1999), CRUNCH (Steefel 2000), and PHAST (Parkhurst et al. 2004). Only a few models allow the velocity field to be internally calculated (e.g., MIN3P, Mayer et al. 2002). Several codes for transient, variably-saturated flow have also been coupled to general biogeochemistry models. These include 3DHYDROGEOCHEM (Yeh and Cheng 1999), TOUGHREACT (Xu et al. 2012), MIN3P (Mayer et al. 2002), HYTEC (Van der Lee et al. 2003), OpenGeoSys-Gem (Kosakowski and Watanabe 2014), and HP1/2/3 (Jacques and Šimůnek 2005; Šimůnek et al. 2013). HP1/2/3, an add-on module to HYDRUS-1D and HYDRUS (2D/3D), and its applications for site remediation and risk assessment of mercury-contaminated sites and for evaluating leaching of uranium from a uranium mine tailings pile will be discussed below.

16.3 Applications of HydroGeoBioChemical Transport Models

16.3.1 Literature Applications

There are many important agricultural and environmental applications for general hydrogeobiochemical models, and many of these appeared in the literature during the last two decades. For example, water leaching from various tailing piles (such as from uranium mills) often contains many trace metals including molybdenum, selenium, arsenic, and chromium (Brookins 1984). Using the HYDROGEOCHEM model, Yeh and Tripathi (1991) simulated the release of trace metals and acidity from an acidic uranium mill tailings pile. Narasimhan et al. (1986) used the DYNAMIX model to study groundwater contamination from an inactive uranium mill tailings pile. Similar studies have been carried out by Walter et al. (1994), Lichtner (1996), and Gerke et al. (1998).

Another significant application for hydrogeobiochemical models is to design and evaluate facilities for the safe disposal and long term isolation of hazardous and radioactive waste, especially high-level nuclear waste. The migration of neptunium between the repository and the ground water table after a hypothetical repository breach at the high-level nuclear waste repository at Yucca Mountain, Nevada, was studied using a multicomponent solute transport model by Viswanathan et al. (1998). The fate of metal-organic mixed wastes was studied by Rittmann and VanBriesen (1996) and VanBriesen (1998). Possible consequences of long term interactions of engineered barriers (clay plugs, concrete components) with the host rock of a disposal facility or various perturbations as a consequence of construction (e.g. oxidation fronts) or waste content are also frequently studied using geochemical transport models (Martens et al. 2010, 2011; Kosakowski and Watanabe 2014). The analysis of redox zone formation in organic-contaminated aquifers was carried out by Abrams et al. (1998) and Essaid et al. (1995), while reactive permeable barriers for aquifer remediation were evaluated by Fryar and Schwartz (1994). Deep geological CO_2 storage (e.g., Gherardi et al. 2012; Walsh et al. 2013) represents another environmental application of reactive transport models. In a study of Jacques et al. (2008a), the transport of major cations and anions and U associated with inorganic P-fertilization were computed for transient flow conditions. This study clearly demonstrated that the distribution coefficient K_d, which is often used to simulate the transport of reactive solutes, may vary significantly during the year as a consequence of transient flow conditions. Thus, the "K_d approach" may represent an inadequate over-simplification of a complex environmental system and may produce erroneous predictions.

Generic multicomponent transport models are sufficiently versatile to allow consideration of soil biological processes such as those involved in the carbon cycle (Jacques et al. 2013), nitrogen cycle (Maggi et al. 2008; Gu et al. 2009), and microbial dynamics (e.g., Thullner et al. 2005; Lim et al. 2007; Centler et al. 2010). For example, Thaysen et al. (2014a, b) implemented the CO_2 module of UnsatChem

into a generic biogeochemical model HP1 and extended it to include the effects of mixed cementitous materials in the soil profile on enhancing inorganic C-leaching to groundwater. Zhang et al. (2013) evaluated the bacterial transport using the HYDRUS-PHREEQC framework and transport parameters depending on solution chemistry.

Although the models with specific chemistry are limited to simulating only the transport and reactions of a limited number of ions (e.g., major ions), there are many important agricultural and environmental problems, such as salinization and sodification of irrigated soils, reclamation of saline or sodic soils, sustainability of various irrigation practices, or the release of saline brine water during mining operations, that can be evaluated using these types of models (Šimůnek and Suarez 1997; Gonçalves et al. 2006; Corwin et al. 2007; Ramos et al. 2011; Rasouli et al. 2013).

Several interesting applications of both the specific and general chemistry models have recently appeared in a special issue of Vadose Zone Journal entitled "Reactive Transport Modeling" (Seaman et al. 2012). The model with specific chemistry was used in a study of Reading et al. (2012), who used the UNSATCHEM code to evaluate the use of gypsum to ameliorate a nonsaline sodic clay soil in North Queensland, Australia. General reactive transport models have been used in the recent studies of Bea et al. (2012), Chang et al. (2012), and Lichtner and Hammond (2012). Bea et al. (2012) used the MIN3P-D multicomponent reactive transport code to describe processes occurring within a mine tailing impoundment and their impact on CO_2 sequestration. Chang et al. (2012) used PHREEQC, in combination with laboratory column experiments, to evaluate the efficacy of Fe(II)-containing solutions as an in-situ means for reducing toxic hexavalent chromium (Cr(VI)) to trivalent chromium (Cr(III)), which subsequently coprecipitates with Fe(III). Lichtner and Hammond (2012) used PFLOTRAN to evaluate geochemical processes controlling the aqueous phase distribution and solid phase speciation of a hexavalent uranium [U(VI)] plume below the Hanford 300 Area bordering the Columbia River in Hanford, WA.

16.3.2 Modeling of Soil Salinity Using the UnsatChem Module of HYDRUS

The UnsatChem geochemical module (Šimůnek and Suarez 1994) simulates the transport of major ions (i.e., Ca^{2+}, Mg^{2+}, Na^{+}, K^{2+}, SO_4^{2-}, CO_3^{2-}, and Cl^{-}) and their equilibrium and kinetic geochemical interactions, such as complexation, cation exchange, and precipitation-dissolution (e.g., of calcite, gypsum and/or dolomite). This module has been implemented into both the one- and two-dimensional computational versions of HYDRUS (Šimůnek et al. 2008). Possible applications of this module include studies of the salinization/reclamation of agricultural soils (Šimůnek and Suarez 1997), sustainability of various irrigation systems (Gonçalves et al. 2006; Ramos et al. 2011; Rasouli et al. 2013), the disposal of brine waters from mining operations, and many other applications (e.g., Schoups et al. 2006; Skaggs et al. 2006; Corwin et al. 2007). Gonçalves et al. (2006) and

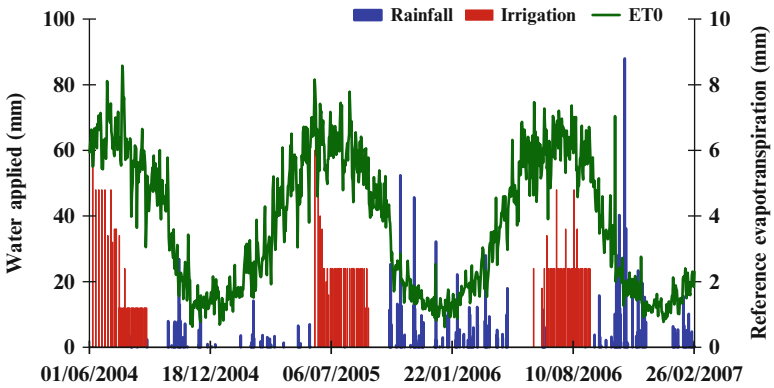

Fig. 16.1 Daily values of precipitation, irrigation and reference evapotranspiration from June 2004 until February 2007

Ramos et al. (2011) recently demonstrated the applicability of UnsatChem to the simulation of the multicomponent transport of major ions both in soil lysimeters and in the field, respectively, irrigated with waters of different quality. They used the UnsatChem module of HYDRUS-1D to describe field measurements of the water content, overall salinity (expressed as Electric Conductivity, EC), the concentration of individual soluble cations, the Sodium Adsorption Ratio (SAR), and the Exchangeable Sodium Percentage (ESP). The experimental data and their analysis using the UnsatChem module are described in detail by Gonçalves et al. (2006) and Ramos et al. (2011) and only selected results from the latter study will be given here.

Problem Description

The field experiment was conducted from June 2004 to February 2007 in the Alentejo region in Southern Portugal on a medium texture soil. The climate in this region is mostly dry, sub-humid to semi-arid, with hot dry summers, and mild winters with irregular rainfall. The experiment involved irrigating maize with either locally available water or with synthetic (with added NaCl) saline water. The experimental field was divided into three groups, A, B, and C (only results for plots A and C are reported below), each having a surface area of 6.75 m^2 (2.25 m wide $\times$ 3 m long; 0.75 m between maize lines), with the Na^+ gradient decreasing from A (saline waters with EC of 7.8 dS m^{-1} during the first two seasons and 15.6 dS m^{-1} during the third season) to C (local water, $EC \leq 1.2$ dS m^{-1}). A drip irrigation system with an overall constant cumulative discharge of 18 L/h/m (24 mm/h) was used to deliver water, salts (NaCl), and fertilizer (N) to the crop. The quality of irrigation water was thus the key variable between plots. The reference evapotranspiration rates (ET_0) were calculated using the Penman-Monteith method. Crop evapotranspiration rates (ET_c) were then calculated using the product of ET_0 and K_c, where K_c is a crop coefficient accounting for both soil evaporation and crop transpiration (Fig. 16.1).

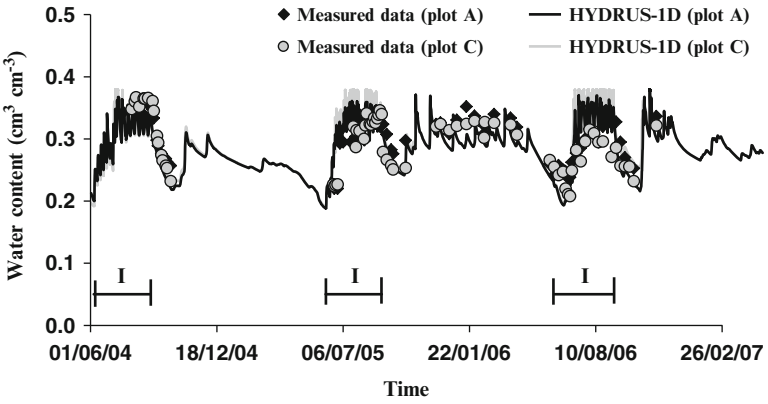

Fig. 16.2 Measured and simulated water contents at a depth of 40 cm. Irrigation seasons are indicated by the letter *I*

TDR probes and ceramic cups were installed at 20, 40, and 60 cm depths to measure soil water contents and collect soil solutions twice a week during irrigation seasons, generally 24 h after an irrigation event, and twice a month during the rest of the year. The soil solution was monitored for the concentrations of soluble Na^+, Ca^{2+}, Mg^{2+}, EC_{sw} (Electrical Conductivity of Soil Water), and *SAR* (Sodium Adsorption Ratio). Soil hydraulic properties for three soil layers were measured using suction tables, the pressure plate apparatus, and the evaporation method on undisturbed soil samples, and fitted using the van Genuchten model. The Gapon selectivity coefficients for four cations (Ca, Mg, K, and Na) were calculated from the initial measured soluble and exchangeable cations concentrations.

Results

Figure 16.2 shows measured and simulated water contents at a depth of 40 cm during the three seasons. During irrigation periods (indicated by a letter I in Fig. 16.2), the amount of water applied in the experimental field was considerably higher than the usual amount of water used to irrigate maize in this region in order to increase water contents above soil field capacity so that soil solution samples could be collected using the installed ceramic cups. As a result, soil water content rapidly increased in the beginning of each irrigation season, and then varied between soil saturation and soil field capacity (Ramos et al. 2011). Between the end of the irrigation seasons (September) and the beginning of rainy seasons (October or November), soil water contents gradually decreased, allowing maize to mature and be harvested. During rainy seasons, soil water contents reflected the occurrence of individual rainfall events (Fig. 16.2).

Figure 16.3 shows that soil salinity increased considerably in the plot irrigated with saline waters. Measured EC_{sw} in plot A reached values higher than 6.0 dS m^{-1}

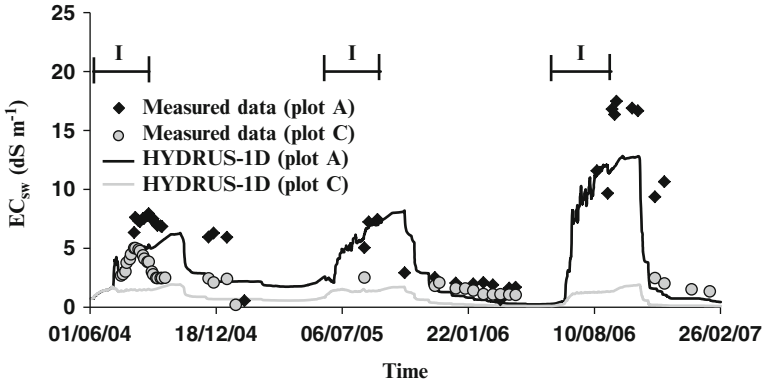

Fig. 16.3 Measured and simulated electrical conductivity of soil water (EC_{sw}) at a depth of 40 cm. Irrigation seasons are indicated by the letter *I*

during the first two irrigation seasons, and higher than 16.0 dS m^{-1} during the third year, as applied water became more saline. In the plot irrigated with the locally available water (plot C), soil salinity remained below 5.0 dS m^{-1} throughout all irrigation seasons. Soil salinity decreased in all plots during rainfall periods, due to soil leaching. Only in the rainy season of 2004–2005, rainfall was not sufficient to completely remove salts from the root zone in plot A, where EC_{sw} values between 2.0 and 6.3 dS m^{-1} were observed in the soil profile (Ramos et al. 2011).

Figure 16.4 shows measured and simulated concentrations of soluble Na^+, Ca^{2+}, and Mg^{2+} for plots A and C at a depth of 40 cm. As the only cation being added to synthetic saline irrigation waters, the general behavior of sodium was similar to EC_{sw}. The highest concentrations were reached in plot A during the irrigation seasons. The highest measured Na^+ concentrations were about 50 $mmol_{(c)}L^{-1}$ during the first 2 years and 130 $mmol_{(c)}L^{-1}$ during the third year. During the rainy seasons, Na^+ concentrations decreased considerably due to soil leaching, similar to EC_{sw}.

The general dynamics of calcium and magnesium concentrations were similar to those of sodium and EC_{sw}. The highest measured Ca^{2+} and Mg^{2+} concentrations were about 20 and 10 $mmol_{(c)}L^{-1}$, respectively. During rainfall events, these values also decreased due to soil leaching. As Ca^{2+} and Mg^{2+} were not added to the synthetic saline irrigation waters applied in plot A, concentrations of these cations in saline waters were the same as in the fresh waters in plot C. Since Na^+ was applied in large concentrations to plot A, both Na^+ concentrations in the soil solution and in the solid phase (not shown) increased, leading to soil sodification. While the exchangeable Na^+ concentration in the solid phase increased, the other cations, namely Ca^{2+} and Mg^{2+}, were inevitably released to the soil solution. For this reason, concentrations of Ca^{2+} and Mg^{2+} were higher in plot A than in plot C where low concentrations of Na^+ were present in the irrigation waters. Since compared to simpler models based on adsorption isotherms, the UnsatChem module is able to consider cation exchange, it was able to simulate the release of Ca^{2+}

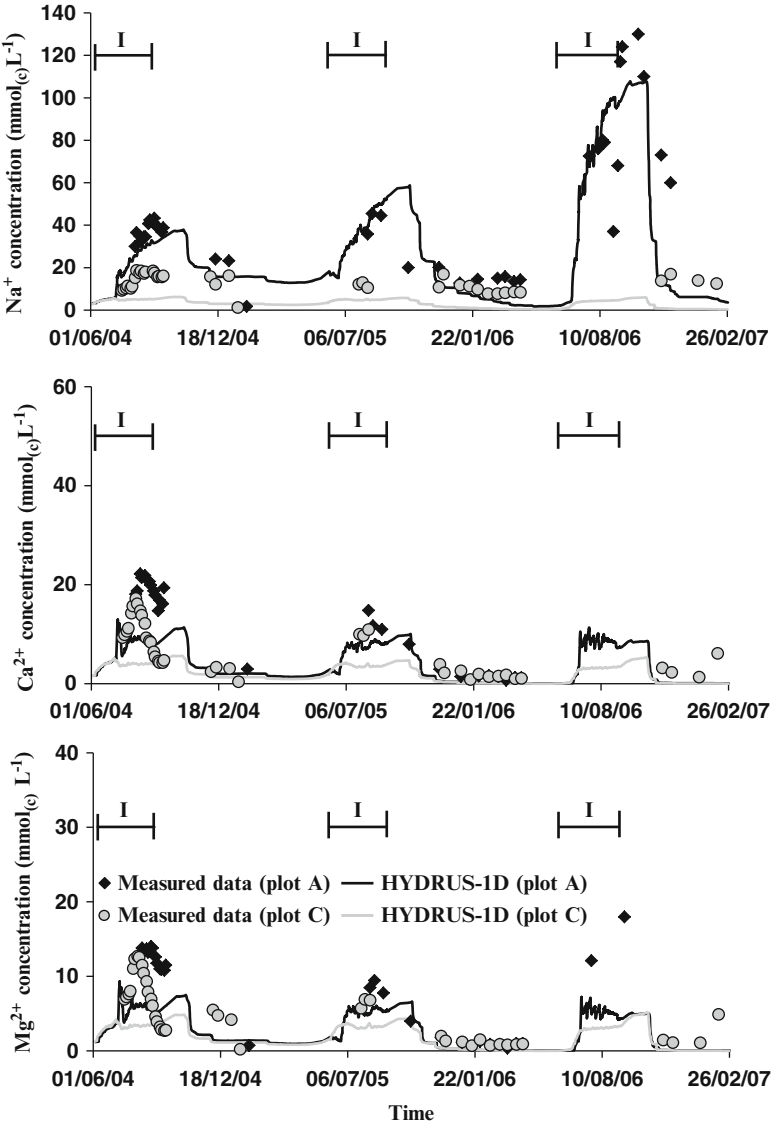

Fig. 16.4 Measured and simulated Na^+ (*top*), Ca^{2+} (*middle*), and Mg^{2+} (*bottom*) concentrations at a depth of 40 cm

and Mg^{2+} from the solid phase as soil sodification increased. The UnsatChem module thus proved to more adequately represent reality than linear models with adsorption isotherms.

Figure 16.5 presents the results for measured and simulated *SAR* values. *SAR* is an integral variable that characterizes salt-affected soils and provides information on comparative concentrations of Na^+, Ca^{2+}, and Mg^{2+} in soil solutions. This variable takes into consideration that the adverse effects of sodium are moderated

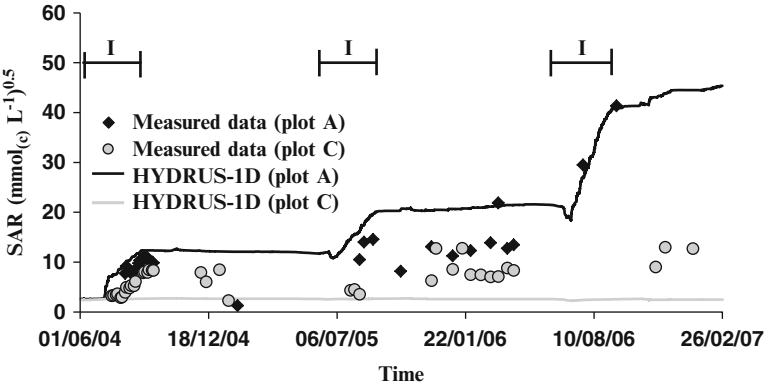

Fig. 16.5 Measured and simulated SAR at a depth of 40 cm

by the presence of calcium and magnesium ions. This makes *SAR* an important variable to consider when managing saline irrigation waters. In plot A, *SAR* increased rapidly in the surface layers after irrigation events, and then also gradually at deeper depths. The application of saline irrigation waters (*SAR* ranged from 38.8 to 80.2 $(\text{mmol}_{(c)}\text{L}^{-1})^{0.5}$) led to very high *SAR* values in the soil solution, reaching about 54 $(\text{mmol}_{(c)}\text{L}^{-1})^{0.5}$ at the end of the experiments. In plot C, irrigated with fresh waters, *SAR* values did not vary significantly, having roughly the same values in the beginning and at the end of the experiments.

Various statistical measures evaluating the goodness of correspondence between the model (the UnsatChem module of HYDRUS-1D) and measurements are given by Ramos et al. (2011) and will not be given here. The correspondence between measurements and model results is very good, considering that most model inputs were independently measured in the laboratory and used in simulations without any further adjustments and/or calibration. The correspondence between measurements and model results obviously could have been better, had the input parameters been calibrated (Ramos et al. 2011). An extensive discussion on the possible causes of deviations between measured data and simulation can also be found in Ramos et al. (2011, 2012).

16.3.3 Modeling the Fate of Mercury in Contaminated Soils Using HP1

The HP1 module, which is used in this example, couples the PHREEQC geochemical code (Parkhurst and Appelo 1999) with HYDRUS-1D (Šimůnek et al. 2008). The one-dimensional version (HP1) was first released in 2005 (Jacques and Šimůnek 2005; Jacques et al. 2008a, b), and used successfully in many applications. HP1, which is an acronym for HYDRUS-PHREEQC-1D, is a relatively comprehensive simulation module that can be used to simulate (1) transient water flow,

(2) the transport of multiple components, (3) mixed equilibrium/kinetic biogeochemical reactions, and (4) heat transport in one-dimensional variably-saturated porous media. HP2 is a corresponding two-dimensional version of HP1, which couples PHREEQC with HYDRUS (2D/3D). Both HP1 and HP2 modules can simulate a broad range of low-temperature biogeochemical reactions in water, the vadose zone and/or ground water systems, including interactions with minerals, gases, exchangers and sorption surfaces based on thermodynamic equilibrium, and kinetic or mixed equilibrium-kinetic reactions.

The example described below illustrates the possibility to simulate the fate of mercury (Hg) in anthropogenic contaminated soil systems (Leterme and Jacques 2013; Leterme et al. 2014).

Problem Definition

Mercury (Hg) poses threats to human health and the environment, notably due to its persistence in the environment and its ability to bioaccumulate in ecosystems (Liu et al. 2012). Mercury pollution can result from either direct contamination (e.g., spills, landfills, mine tailings) or indirect pathways, such as atmospheric deposition (Guédron et al. 2013). Mercury mining, gold and silver mining, manufacturing (chlor-alkali plants, manometer spill), wood preservation and cemeteries (through the release of Hg from dental amalgams) have been identified as the main sources of soil contamination (UNEP 2002). In addition, Hg geochemistry is quite complex (Fig. 16.6) and thus Hg contamination can occur in different forms: as aqueous inorganic and organic Hg^{II} species, in elemental form (Hg^0) in a (residual) non-aqueous liquid phase (NAPL), or as a solid phase (e.g., cinnabar). Hg transport is highly influenced by its strong binding to organic matter, especially to the thiol groups, which decreases (sorption to soil organic matter) or increases (complexation with dissolved organic matter) the mobility of mercury. Reduction of Hg^{II} to Hg^0 enhances the Hg transport through the gaseous phase, which is an important pathway in mercury-related risk assessment studies. Note that under reducing conditions, organic forms of mercury (monomethylmercury and dimethylmercury) may occur and may have a strong tendency for bioaccumulation in wetland systems.

Leterme et al. (2014) implemented the conceptual model presented in Fig. 16.6 into HP1. This model addresses Hg-contaminated soils under oxidizing conditions (organic forms of Hg are excluded). They investigated seven scenarios with initial conditions representing different types of contamination (cinnabar, residual NAPL, and aqueous Hg^{II}, and any combination of these three contamination sources) polluting the first 10 cm of the soil (Fig. 16.7). Only the first three scenarios are presented below. They also evaluated the sensitivity of four different indicators, illustrated in Fig. 16.7, to different parameters and processes.

Daily climatic data (50 years) at Dessel, Belgium, were used to define surface atmospheric boundary conditions and free drainage was considered as the bottom boundary condition (representing deep groundwater and oxidising conditions).

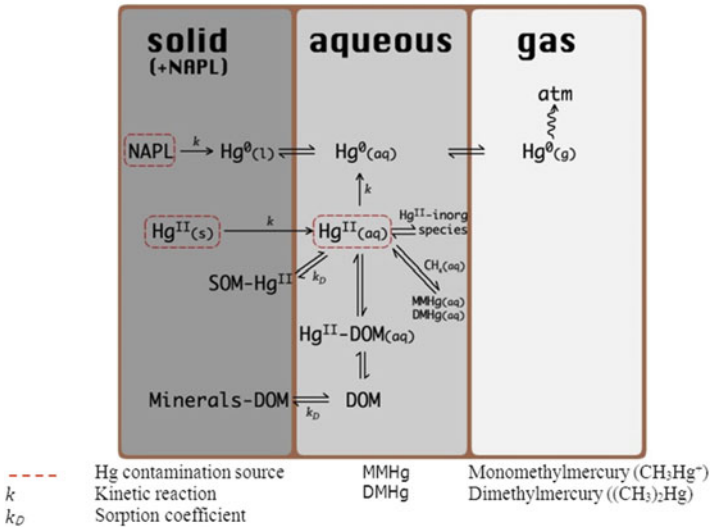

Fig. 16.6 Conceptual model of Hg speciation and reactions in soil systems (*DOM* dissolved organic matter, *SOM* soil organic matter, *MMHg* monomethylmercury, *DMHg* dimethylmercury)

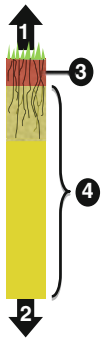

#	Indicator
1	Percentage of Hg volatilized to atmosphere
2	Percentage of Hg leached out of the soil profile
3	Percentage of Hg present in the originally-polluted soil horizon (top 10 cm)
4	Percentage of Hg present in the soil profile (10-100 cm) below the originally-polluted soil horizon

Fig. 16.7 Problem definition and evaluated indicators. Initial Hg contamination is in the first 10 cm of the soil (*red shaded*). The top 30 cm of the soil contains soil organic matter (*grey shaded*), the remaining part of the soil profile is inert

Incoming water has a typical rain water composition and contains dissolved organic matter (DOM). Soil texture is sandy (this a priori corresponds to coarse-textured soil types, likely to be encountered at polluted sites such as mine tailings) with a grass cover (30 cm rooting depth). Soil organic matter (SOM) and the initial Hg contamination are uniform in the top 30 and 10 cm of the soil profile, respectively. There is a background atmospheric Hg(g) concentration of 1 ng m^{-3}. Soil and dissolved organic matter are both represented by four different reactive sites (three representing oxygen sites of fulvic and humic acids and one representing thiols).

Results

Figure 16.8 shows depth profiles of the initial contamination source and Hg concentrations sorbed to SOM for three contamination scenarios and selected times (initial, and 5, 10, 25, and 50 years). Since the dissolution rate of cinnabar is relatively slow, about 50 % of the initial amount still remains after 50 years (Fig. 16.8, top). Note the non-uniform dissolution profile of cinnabar due to the dependence of the dissolution kinetics on DOM concentrations. Because of the slow dissolution rate of cinnabar and the presence of the strongly binding DOM thiols, almost no Hg is retained on the SOM in the first few centimetres of the soil. As DOM thiols move downward through the contaminated zone (top 10 cm), they are increasingly more saturated with mercury due to continued cinnabar dissolution, and more Hg is retained by SOM, resulting in a peak retention of Hg at the bottom of the initially polluted soil layer (Fig. 16.8, top).

In the scenario with residual NAPL (Fig. 16.8, middle), all elemental Hg is dissolved after about 10 years. Because of this gradual release, mercury is mostly retained within the top 10 cm during the first 25 years. Since the release of Hg from NAPL is fast enough to saturate the thiol groups of DOM, a significant portion of mercury is retained on SOM. After 25 years, the gradual leaching of mercury to the lower soil horizons is obvious.

In the scenario with initial aqueous contamination (Fig. 16.8, bottom), a large portion of Hg leaches very quickly (mainly in the form of inorganic species such as $Hg(OH)_2$, $HgCl_2$, HgOCl) from the top 10 cm and sorbs significantly to the SOM in the underlying 20 cm. Note that the "Initial" concentration profile is drawn after the first time step, which explains the "Initial" profile of Hg sorbed to SOM. Also from the start, all Hg is available for leaching via complexation on the thiols of DOM (although binding is much stronger on the thiols of DOM than of SOM, their capacity, i.e., the number of thiol sites, is very limited), resulting in a gradual leaching of Hg from the top 10 cm.

Figure 16.9 shows Hg^{II} fluxes from the top 1 m to underlying layers for the first 25 years of the simulations. A quick initial release of mobile Hg in the scenario with a $HgCl_2$(aq) contamination (a green line in Fig. 16.9) leads to earlier Hg leaching than in scenarios with cinnabar and NAPL contaminations (red and blue lines, respectively). In these two scenarios, Hg leaching occurs only after a few years, but remains at only about half of the Hg flux in the scenario with the $HgCl_2$(aq) contamination. This is because in the latter case Hg was rapidly redistributed in the top 30 cm (Fig. 16.8, bottom right) and less re-sorption occurs when it complexes with DOM thiols. Hg fluxes for scenarios with cinnabar and Hg NAPL are quite similar because the limiting factor for Hg mobility is not the Hg release through dissolution nor the sorption capacity of the soil solid phase, but rather the availability of DOM thiol groups. Figure 16.9 also shows that the temporal dynamics (not its absolute values) of leaching is driven by the climate.

The sensitivity analysis indicated that the most sensitive parameters are related to SOM and DOM. DOM concentration strongly influence the mobility and

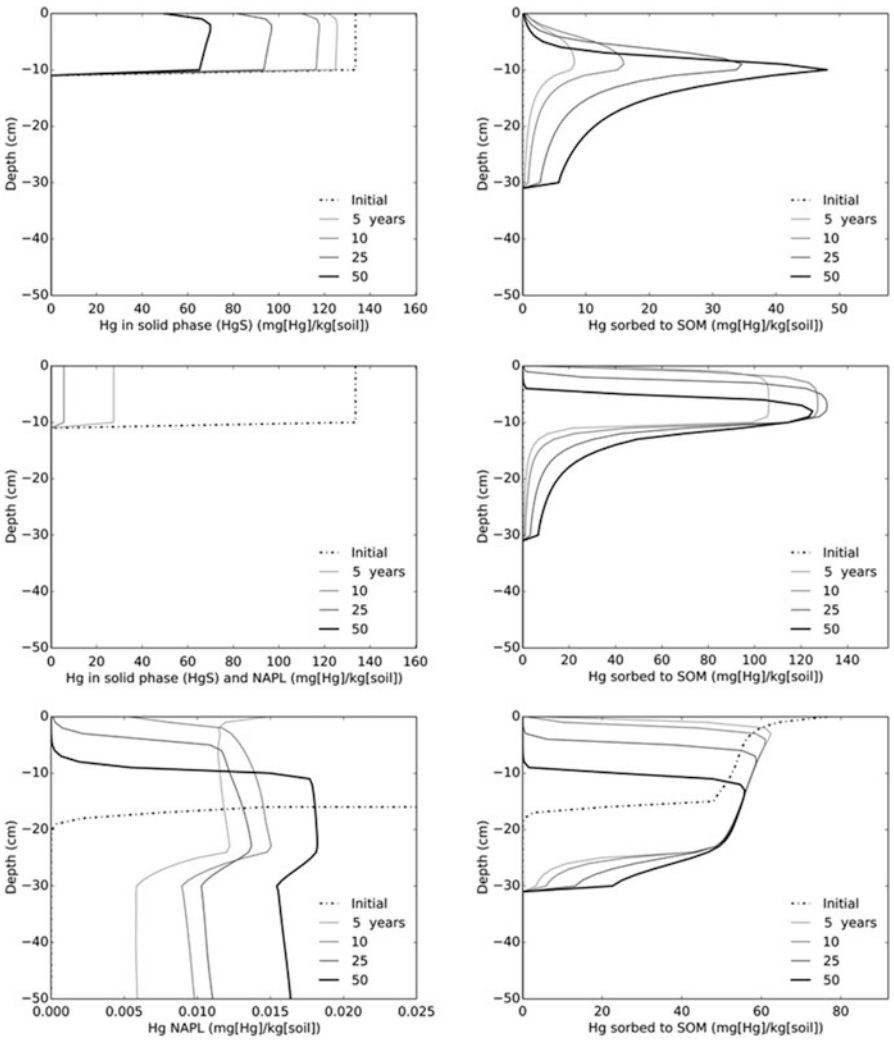

Fig. 16.8 Depth profiles at selected times for different forms of Hg for different types of initial contamination: cinnabar (*top*), residual NAPL (*middle*), and aqueous Hg species (*bottom*). The *left column* shows Hg concentrations of the original contamination, the *right columns* shows Hg sorbed to SOM. Note different scales of the x-axis

leaching of mercury due to the high affinity of Hg to DOM thiol groups. On the other hand, the exchange capacities and the selectivity coefficients of the fulvic and humic acids of SOM greatly influence the retention of mercury in the top soil. Note also that the selectivity coefficient of the thiol groups in SOM has only a minor effect because in anthropogenic mercury-contaminated sites, the thiol groups in SOM are initially saturated with mercury. The dissolution rate of the initial

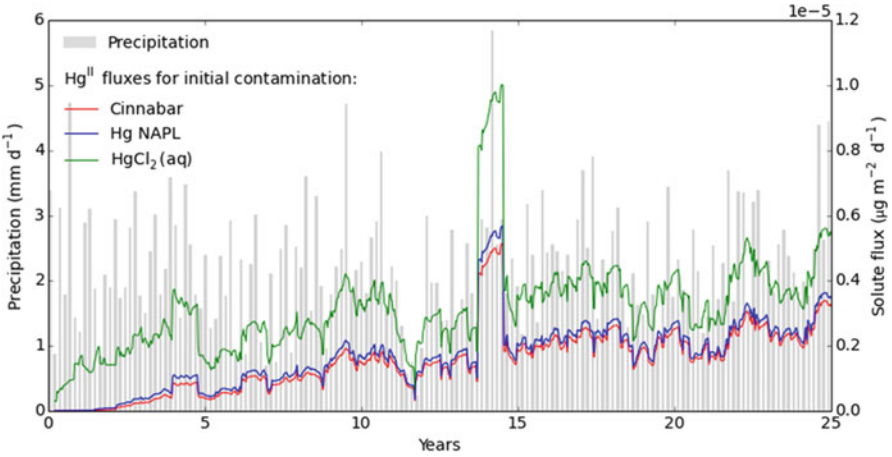

Fig. 16.9 Precipitation (*left axis*) and Hg^{II} fluxes (monthly moving averages) at the bottom of the soil profile for three initial contamination scenarios (*right axis*)

contamination is also a sensitive parameter as illustrated above in scenarios with cinnabar and residual NAPL.

16.3.4 Modeling of Uranium Leaching from a U Tailings Pile Using the HP2 Module of HYDRUS (2D/3D)

The HP2 is a two-dimensional equivalent of the one-dimensional HP1 program (Šimůnek et al. 2008). We will demonstrate below the versatility of HP2 using an example involving the release and migration of uranium from a simplified uranium mill tailings pile toward a river. This example includes the processes of water flow, solute transport, precipitation/dissolution of the solid phase, cation exchange, complexation, and many other reactions. This problem was inspired by, and is a modification of (to make it more realistic), a problem reported by Yeh and Tripathi (1991). Detailed information about this project, as well as instructions on how to implement the project using HP2, can be found in Šimůnek et al. (2012) and on the HYDRUS website.

Problem Description

The schematic of the transport domain is shown in Fig. 16.10. The mill tailings pile is located adjacent to a surface that slopes down to a river. The horizontal bottom of the region is impermeable. The vertical left-edge has the Dirichlet boundary

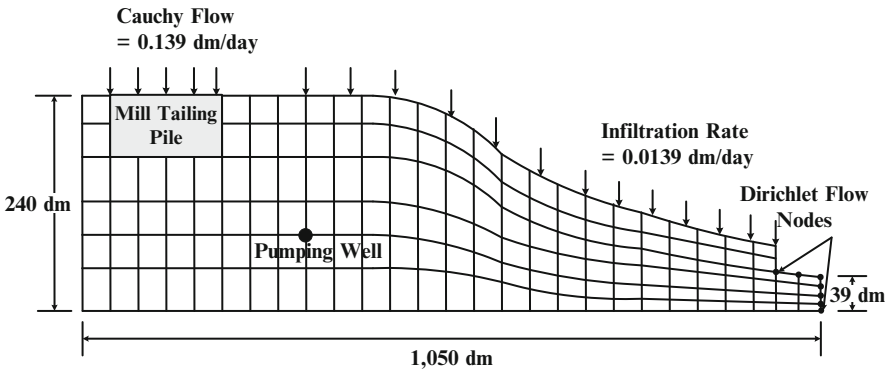

Fig. 16.10 Problem description for the uranium tailings problem (Adopted from Yeh and Tripathi 1991)

condition with a groundwater table 12 m above the bottom of the transport domain. The top boundary (except for the mill tailings pile and the river) has a flux boundary condition with a net rainfall rate of 0.139 cm/day. The horizontal region on the top of the mill tailings pile is a flux boundary with an infiltration rate of 1.39 cm/day. The nodes on the vertical line on the right side of the transport domain and the nodes on the river bottom have the Dirichlet boundary condition, reflecting the position of water in the river (4.5 m above the bottom of the transport domain). A hypothetical pumping well with a withdrawal rate of 271.58 cm^2/day is located at $(x, z) = (400, 100)$. The region is discretized using a structured finite element mesh with 1,564 elements and 852 nodes.

The medium has the hydraulic properties of a loam (the residual water content, $\theta_r = 0.078$, the saturated water content, $\theta_s = 0.430$, and the van Genuchten (1980) parameters $\alpha = 0.036$ cm^{-1}, and $n = 1.56$; Carsel and Parrish 1988) with the saturated hydraulic conductivity of $K_s = 3.78$ m/day. A longitudinal dispersivity of 2.5 m and a transverse dispersivity of 0.25 m are assumed.

With respect to solute transport, uranium was modeled as a complex multicomponent system involving multiple interacting components. Table 16.1 lists chemical reactions and their thermodynamic equilibrium constants considered in this example. For reactive hydrogeochemical transport, the problem consists of eight components: Total H, Total O, Ca, C, uranium, sulfate, phosphate, and Fe. A total of 35 aqueous species, 18 exchange species, 9 surface species and 2 minerals are defined for the problem; redox reactions were not considered. Precipitation/dissolution and sorption are the main chemical processes considered in this example. Gypsum (0.0037 mol/kg) and calcite (0.00047 mol/kg) are assumed to be present in the waste zone and the rest of the profile, respectively.

Sorption of U was described using a multi-site cation exchange model (see Jacques et al. 2008a). This sorption model also buffers the acid pH due to proton exchange. In the current model, protons will replace Ca in the exchange complex. Parameters of the multi-site cation exchange model are also given in Table 16.1 (adapted from Jacques

Table 16.1 Reaction network for the uranium tailings pile leaching problem

Reaction	No.	Log K[a]
Aqueous complexation reactions		
$H_2O \Leftrightarrow H^+ + OH^-$	(R1)	−14.00
$Ca^{2+} + CO_3^{2-} \Leftrightarrow CaCO3\ (aq)$	(R2)	3.22
$Ca^{2+} + H^+ + CO_3^{2-} \Leftrightarrow CaHCO_3^+$	(R3)	11.43
$Ca^{2+} + SO_4^{2-} \Leftrightarrow CaSO_4\ (aq)$	(R4)	2.31
$Ca^{2+} + 2H^+ + PO_4^{3-} \Leftrightarrow CaH^2PO_4^+$	(R5)	20.96
$Ca^{2+} + PO_4^{3-} \Leftrightarrow CaPO_{4-}$	(R6)	6.46
$Ca^{2+} + H^+ + PO_4^{3-} \Leftrightarrow CaHPO_{4\ (aq)}$	(R7)	15.08
$Ca^{2+} + H_2O \Leftrightarrow H^+ + CaOH^+$	(R8)	−12.58
$Fe^{2+} + SO_4^{2-} \Leftrightarrow FeSO_{4\ (aq)}$	(R9)	2.20
$Fe^{2+} + H_2O \Leftrightarrow H^+ + FeOH^+$	(R10)	−9.50
$Fe^{2+} + 2H_2O \Leftrightarrow 2H^+ + Fe(OH)_{2\ (aq)}$	(R11)	−20.57
$Fe^{2+} + 3H_2O \Leftrightarrow 3H^+ + Fe(OH)_3^-$	(R12)	−31.00
$Fe^{2+} + 4H_2O \Leftrightarrow 4H^+ + Fe(OH)_4^{2-}$	(R13)	−43.00
$UO_2^{2+} + H_2O \Leftrightarrow H^+ + (UO_2)(OH)^+$	(R14)	−5.30
$2UO_2^{2+} + 2H_2O \Leftrightarrow 2H^+ + (UO2)_2(OH)_2^{2+}$	(R15)	−5.68
$3UO_2^{2+} + 4H_2O \Leftrightarrow 4H^+ + (UO2)_3(OH)_4^{2+}$	(R16)	−11.88
$3UO_2^{2+} + 5H_2O \Leftrightarrow 5H^+ + (UO2)_3(OH)_5^+$	(R17)	−15.82
$4UO_2^{2+} + 7H_2O \Leftrightarrow 7H^+ + (UO2)_4(OH)_7^+$	(R18)	−21.90
$3UO_2^{2+} + 7H_2O \Leftrightarrow 7H^+ + (UO_2)_3(OH)_7^-$	(R19)	−28.34
$UO_2^{2+} + CO_3^{2-} \Leftrightarrow (UO_2)(CO_3)_{(aq)}$	(R20)	9.65
$UO_2^{2+} + 2CO_3^{2-} \Leftrightarrow (UO_2)(CO_3)_2^{2-}$	(R21)	17.08
$UO_2^{2+} + 3CO_3^{2-} \Leftrightarrow (UO_2)(CO_3)_3^{4-}$	(R22)	21.70
$2UO_2^{2+} + CO_3^{2-} + 3H_2O \Leftrightarrow 3H^+ + (UO_2)_2(CO_3)(OH)_3^-$	(R23)	−1.18
$UO_2^{2+} + SO_4^{2-} \Leftrightarrow (UO_2)(SO_4)_{\ (aq)}$	(R24)	2.95
$UO_2^{2+} + 2SO_4^{2-} \Leftrightarrow (UO_2)(SO_4)_2^{2-}$	(R25)	4.00
$2H^+ + UO_2^{2+} + PO_4^{3-} \Leftrightarrow H_2(UO_2)(PO_4)^+$	(R26)	23.20
$3H^+ + UO_2^{2+} + PO_4^{3-} \Leftrightarrow H_3(UO_2)(PO_4)^{2+}$	(R27)	22.90
$Ca^{2+} + 4H^+ + UO_2^{2+} + 2PO_4^{3-} \Leftrightarrow CaH_4(UO_2)(PO_4)_2^{2+}$	(R28)	45.24
$Ca^{2+} + 5H^+ + UO_2^{2+} + 2PO_4^{3-} \Leftrightarrow CaH_5(UO_2)(PO_4)_2^{3+}$	(R29)	46.00
$H^+ + CO_3^{2-} \Leftrightarrow HCO_3^-$	(R30)	10.32
$2H^+ + CO_3^{2-} \Leftrightarrow H_2CO_{3(aq)}$	(R31)	16.67
$H^+ + SO_4^{2-} \Leftrightarrow HSO_4^-$	(R32)	1.99
$H^+ + PO_4^{3-} \Leftrightarrow HPO_4^{2-}$	(R33)	12.35
$2H^+ + PO_4^{3-} \Leftrightarrow H_2PO_4^-$	(R34)	19.55
$3H^+ + PO_4^{3-} \Leftrightarrow H_3PO4$	(R35)	21.74
Precipitation-dissolution reactions		
$Ca^{2+} + SO_4^{2-} \Leftrightarrow CaSO_{4(s)}\ (gypsum)$	(R36)	4.62
$Ca^{2+} + CO_3^{2-} \Leftrightarrow CaCO_{3(s)}\ (calcite)$	(R37)	8.48
Multi-site cation exchange model[b]		
$Ca^{2+} + 2\ Y_i^- = CaY_{i2}$	(R37)	−0.2
$UO_2^{2+} + 2\ Y_i^- = UO2Y_{i2}$	(R38)	−0.2
$H^+ + Y_a = HY_a$	(R39)	1.65
$H^+ + Y_b = HY_b$	(R40)	3.30
$H^+ + Y_c = HY_c$	(R41)	4.95
$H^+ + Y_d = HY_d$	(R42)	6.85
$H^+ + Y_e = HY_e$	(R43)	9.60
$H^+ + Y_f = HY_f$	(R44)	12.35

(continued)

Table 16.1 (continued)

Reaction	No.	Log K[a]
Specific sorption – surface complexation		
$Hfo\_OH + H^+ = Hfo\_OH_2^+$	(R45)	7.29
$Hfo\_OH = Hfo\_O^- + H^+$	(R46)	−8.93
$Hfo\_OH + Ca^{2+} = Hfo\_OCa^+ + H^+$	(R47)	−5.85
$Hfo\_OH + UO_2^{2+} = Hfo\_OUO_2^+ + H^+$	(R48)	2.8
$Hfo\_OH + PO_4^{3+} + 3H^+ = Hfo\_H_2PO_4 + H_2O$	(R49)	31.29
$Hfo\_OH + PO_4^{3+} + 2H^+ = Hfo\_HPO_4^- + H_2O$	(R50)	25.39
$Hfo\_OH + PO_4^{3+} + H^+ = Hfo\_PO_4^{2-} + H_2O$	(R51)	17.72
$Hfo\_OH + SO_4^{2-} + H^+ = Hfo\_SO_4^- + H_2O$	(R52)	7.78
$Hfo\_OH + SO_4^{2-} = Hfo\_OHSO_4^{-2}$	(R53)	0.79

[a]*K* is a thermodynamic equilibrium constant
[b]Y_i represents one of the six different exchange sites (Y_a, Y_b, Y_c, Y_d, Y_e, Y_f). Exchange coefficients are the same for each exchange site for Ca^{2+} and UO_2^{2+}, but are different for H^+

Table 16.2 Initial and boundary compositions of recharge water and pore water in the tailings and regions outside of the tailings for the uranium tailings problem (mol/l)

Species	Inside the tailings	Outside the tailings
Ca^{2+}	1.14×10^{-2}[a]	1.42×10^{-2}[a]
CO_3^{2-}	1.0×10^{-2}	1.5×10^{-3}
UO_2^{2+}	5.0×10^{-4}	1.0×10^{-7}
PO_4^{3-}	1.0×10^{-6}	7.5×10^{-7}[b]
SO_4^{2-}	5.33×10^{-2}[c]	1.35×10^{-2}[d]
Fe^{2+}	3.5×10^{-2}	1.0×10^{-7}
pH	2.3	7.14[c]

[a]Calculated in equilibrium with calcite
[b]Calculated slightly under-saturated with hydroxyapatite (the saturation index of −0.1)
[c]Used as charge balance
[d]Calculated slightly under-saturated with gypsum (the saturation index of −0.1)

et al. 2008a). A relatively low (8.1×10^{-3} mol/kg) sorption capacity and a bulk density of 1.5 g/cm^3 were considered. Additionally, specific sorption of U and other cations and anions on Fe-oxides were described using a non-electrostatic surface complexation model with a capacity of 8.1×10^{-4} mol/kg. Parameters of this non-electrostatic surface complexation model are also given in Table 16.1.

Two different water compositions were considered: (i) one solution composition was considered for pore water and recharge water in the tailings, and (ii) the second solution composition was used for pore water and recharge water outside of the tailings pile and for recharge water at the left hand side of the domain. Both water types are given in Table 16.2. Cauchy boundary conditions were considered on all boundaries where boundary conditions are specified. A total of 1,000 days was simulated.

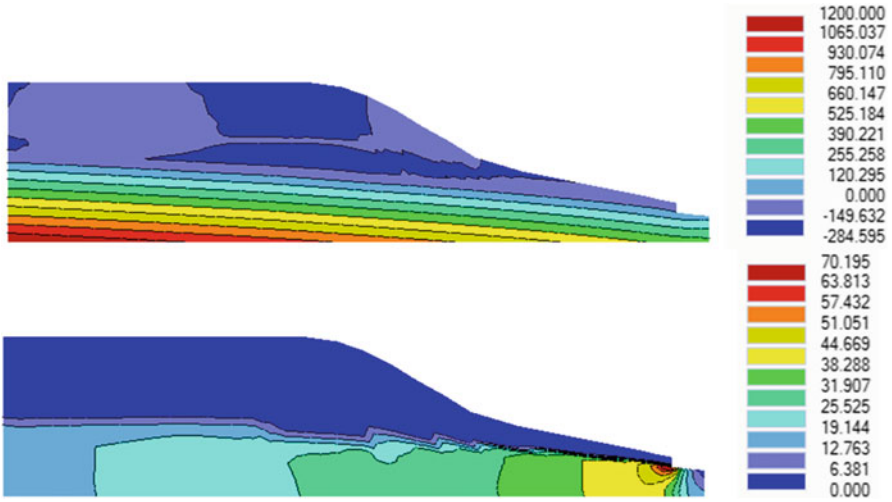

Fig.16.11 The steady-state pressure head (cm) (*top*) and flux (cm/d) (*bottom*) profiles (at 1,000 days) for the tailings pile leaching example

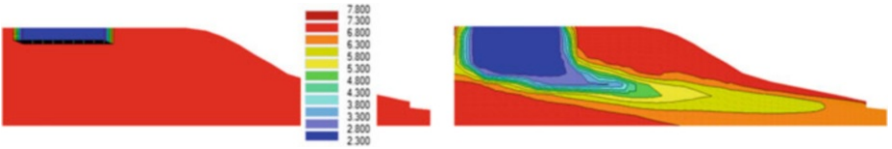

Fig. 16.12 Spatial distribution of pH initially (*left*) and at 1,000 days (*right*) for the tailings pile leaching example

Results

The steady-state pressure heads and velocity fields are depicted in Fig. 16.11. Figure 16.11 shows that water fluxes in the groundwater (about 20-50 cm/day) were significantly larger than in the vadose zone (below 1.5 cm/day).

Figure 16.12 shows contour plots of the initial (left) and final (right) distributions of pH. Acidity was initially confined to the tailings pile and was larger than 7 outside of the tailings pile. The proton exchange on the cation exchanger buffered the acidity by replacing calcium with protons on the exchanger. The spatial extent of the pH-altered region extended all the way to the river.

Figure 16.13 depicts contour plots of precipitated carbonate (Calcite, $CaCO_{3(s)}$) and sulfate (Gypsum, $CaSO_{4(s)}$) at 1,000 days. $CaCO_{3(s)}$, which was initially present everywhere outside of the tailings, is dissolved completely in the zone where pH is lower than about 5.5 (see Fig. 16.12). The influence of the acidity on calcite precipitation is present almost in the entire domain, except for the upper right and bottom left parts of the domain. In these zones, the geochemistry was governed by incoming rain water (upper part) or ground water (bottom left). Dissolution of

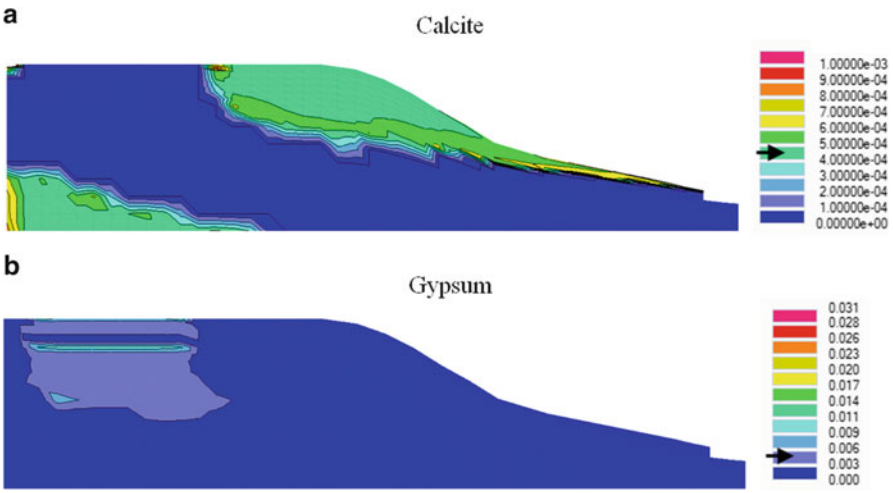

Fig. 16.13 Spatial distribution of calcite (**a**) and gypsum (**b**) at 1,000 days for the tailings pile leaching example. *Arrows* indicate the color representing the initial conditions for calcite in the soil region or for gypsum in the tailings pile

Fig. 16.14 Spatial distribution of aqueous U concentration (mol/l) at 1,000 days

Fig. 16.15 Spatial distribution of sorbed U concentration (mol/dm^3) at 1,000 days

calcite and the abundance of sulphate in tailings water led to gypsum precipitation. Gypsum, which was initially present only inside of the tailings, precipitated in the domain where groundwater encountered the leachate from the tailings.

Figures 16.14 and 16.15 show dissolved and sorbed uranium concentration profiles, respectively, as calculated using HP2 (i.e., using complex biogeochemical calculations). U migration within the ground water system is considerably retarded. U sorption seems to coincide quite well with the downstream edge of the aqueous U plume.

16.4 Conclusions

In spite of the considerable demand on input data, the multicomponent solute transport models such as HYDRUS, UnsatChem, or HP1/2, can be effective and versatile tools that are very useful for evaluating complex agricultural and environmental problems, such as irrigation management in regions with scarce water resources, where suitable waters are not always available for irrigation or for evaluating the leaching of acidic waters from mine tailings. We have demonstrated the use of the UnsatChem and HP2 modules of the HYDRUS software for these two types of applications, respectively. These models, after proper calibration and validation, should be considered useful tools for establishing sound irrigation and environmental policies to mitigate various problems such as soil salinization/sodification or point and non-point source pollution from mining operations. Additional examples of the use of the complex hydrobiogeochemical transport models can be found at (and downloaded from) the HYDRUS website.

References

Abrams RH, Loague K, Kent DB (1998) Development and testing of a compartmentalized reaction network model for redox zones in contaminated aquifers. Water Resour Res 34:1531–1541

Ahuja LR, Hebson C (1992) Root zone water quality model. GPSR Tech. Rep. No. 2. USDA, ARS, Fort Collins

Bea SA, Wilson SA, Mayer KU, Dipple GM, Power IM, Gamazo P (2012) Reactive transport modeling of natural carbon sequestration in ultramafic mine tailings. Vadose Zone J 11(2). doi:10.2136/vzj2011.0053

Bell LSJ, Binning PJ (2004) A split operator approach to reactive transport with the forward particle tracking Eulerian-Lagrangian localized adjoint method. Adv Water Resour 27:323–334

Brookins DG (1984) Geochemical aspects of radioactive waste disposal. Springer, New York

Carsel RF, Parrish RS (1988) Developing joint probability distributions of soil water retention characteristics. Water Resour Res 24:755–769

Centler F, Shao H, De Biase C, Park C-H, Regnier P, Kolditz O, Thullner M (2010) GeoSysBRNS – a flexible multidimensional reactive transport model for simulating biogeochemical subsurface processes. Comput Geosci 36:397–405

Chang H, Singer JH, Seaman JC (2012) In situ chromium(VI) reduction using iron(II) solutions: modeling dynamic geochemical gradients. Vadose Zone J 11(2). doi:10.2136/vzj2011.0172

Corwin DL, Rhoades JD, Šimůnek J (2007) Leaching requirement for soil salinity control: steady-state vs. transient-state models. Agric Water Manage 90(3):165–180

Essaid HI, Bekins BA, Godsy EM, Warren E, Baedecker MJ, Cozzarelli IM (1995) Simulation of aerobic and anaerobic biodegradation processes at a crude oil spill site. Water Resour Res 31(12):3309–3327

Fryar AE, Schwartz FW (1994) Modeling the removal of metals from groundwater by a reactive barrier: experimental results. Water Resour Res 30(12):3455–3469

Gerke HH, Molson JW, Frind EO (1998) Modelling the effect of chemical heterogeneity on acidification and solute leaching in overburden mine spoils. J Hydrol 209:166–185

Gherardi F, Audigane P, Gaucher EC (2012) Predicting long-term geochemical alteration of wellbore cement in a generic geological CO_2 confinement site: tackling a difficult reactive transport modeling challenge. J Hydrol 420–421:340–359

Gonçalves MC, Šimůnek J, Ramos TB, Martins JC, Neves MJ, Pires FP (2006) Multicomponent solute transport in soil lysimeters irrigated with waters of different quality. Water Resour Res 42:W08401, 17 pp. doi:10.1029/2006WR004802

Gu CH, Maggi F, Riley WJ, Hornberger GM, Xu T, Oldenburg CM, Spycher N, Miller NL, Venterea RT, Steefel C (2009) Aqueous and gaseous nitrogen losses induced by fertilizer application. J Geophys Res 114, G01006

Guédron S, Grangeon S, Jouravel G, Charlet L, Sarret G (2013) Atmospheric mercury incorporation in soils of an area impacted by a chlor-alkali plant (Grenoble, France): contribution of canopy uptake. Sci Total Environ 445–446:356–364

Hutson JL, Wagenet RJ (1992) LEACHM: leaching estimation and chemistry model. Research series no. 92-3, Cornell University, Ithaca

Jacques D, Šimůnek J (2005) User manual of the multicomponent variably-saturated flow and transport model HP1, description, verification and examples, version 1.0, SCK•CEN-BLG-998, Waste and disposal. SCK•CEN, Mol, 79 pp

Jacques D, Šimůnek J, Mallants D, van Genuchten MT (2006) Operator-splitting errors in coupled reactive transport codes for transient variably saturated flow and contaminant transport in layered soil profiles. J Contam Hydrol 88:197–218

Jacques D, Šimůnek J, Mallants D, van Genuchten MT (2008a) Modeling coupled hydrological and chemical processes: long-term uranium transport following mineral phosphorus fertilization. Vadose Zone J 7(2):698–711. doi:10.2136/VZJ2007.0084

Jacques D, Šimůnek J, Mallants D, van Genuchten MT (2008b) Modelling coupled water flow, solute transport and geochemical reactions affecting heavy metal migration in a podzol soil. Geoderma 145:449–461

Jacques D, Šimůnek J, Mallants D, van Genuchten MTh (2013) The HPx reactive transport models: summary of recent developments and applications. In: Šimůnek J, van Genuchten MTh, Kodešová R (eds) Proceedings of the 4th international conference HYDRUS software applications to subsurface flow and contaminant transport problems. Invited paper, 21–22 Mar 2013. Department of Soil Science and Geology, Czech University of Life Sciences, Prague. ISBN: 978-80-213-2380-3, pp 7–16

Jansson P-E, Karlberg L (2001) Coupled heat and mass transfer model for soil-plant-atmosphere systems. Royal Institute of Technology, Department of Civil and Environmental Engineering, Stockholm, 325 pp

Kosakowski G, Watanabe N (2014) OpenGeoSys-Gem: a numerical tool for calculating geochemical and porosity changes in saturated and partially variable saturated media. Phys Chem Earth (in press). doi:http://dx.doi.org/10.1016/j.pce.2013.11.008

Langergraber G, Šimůnek J (2005) Modeling variably-saturated water flow and multi-component reactive transport in constructed wetlands. Vadose Zone J 4(4):924–938

Langergraber G, Šimůnek J (2012) Reactive transport modeling of subsurface flow constructed wetlands. Vadose Zone J 11(2). doi:10.2136/vzj2011.0104, 14 pp

Leij FJ, Bradford SA (1994) 3DADE: a computer program for evaluating three-dimensional equilibrium solute transport in porous media. Research report no. 134. U. S. Salinity Laboratory, USDA, ARS, Riverside

Leterme B, Jacques D (2013) Modeling Hg reactive transport in soil system using HP1. In: Šimůnek J, van Genuchten MTh, Kodešová R (eds) Proceedings of the 4th international conference HYDRUS software applications to subsurface flow and contaminant transport problems. Invited paper, 21–22 Mar 2013. Department of Soil Science and Geology, Czech University of Life Sciences, Prague. ISBN: 978-80-213-2380-3, pp 225–234

Leterme B, Blanc P, Jacques D (2014) A reactive transport model for mercury fate in soils – application to different anthropogenic pollution sources. Soil Pollut (in review)

Lichtner PC (1996) Continuum formulation of multicomponent-multiphase reactive transport. In: Lichtner PC, Steefel CI, Oelkers EH (eds) Reactive transport in porous media, reviews in mineralogy, Chapter 1, vol 34. Mineralogical Society of America, Washington, DC, pp 1–81

Lichtner PC, Hammond GE (2012) Using high performance computing to understand roles of labile and nonlabile uranium(VI) on Hanford 300 area plume longevity. Vadose Zone J 11(2). doi:10.2136/vzj2011.0097

Lim M-S, Yeo IW, Clement TP, Roh Y, Lee K-K (2007) Mathematical model for predicting microbial reduction and transport of arsenic in groundwater systems. Water Res 41:2079–2088

Liu G, Cai Y, O'Driscoll N, Feng X, Jiang G (2012) Overview of mercury in the environment. In: Liu G, Cai Y, O'Driscoll N (eds) Environmental chemistry and toxicology of mercury. Chantilly, VA, pp 1–12

Maggi F, Gu C, Riley WJ, Venterea R, Hornberger GM, Venterea RT, Xu T, Spycher N, Steefel C, Miller NL, Oldenburg CM (2008) A mechanistic treatment of the dominant soil nitrogen cycling processes: model development, testing, and application. J Geophys Res Biogeosci 113, G02016. doi:10.1029/2007JG000578

Mangold DC, Chin-Fu Tsang (1991) A summary of subsurface hydrological and hydrochemical models. Rev Geophys 29(1):51–79

Martens E, Jacques D, Van Gerven T, Wang L, Mallants D (2010) Geochemical modelling of leaching of Ca, Mg, Al, and Pb from cementitious waste forms. Cement Concr Res 40(8):1298–1305

Martens E, Jacques D, Wang L, De Cannière P, Moors H, Van Gompel M, Mariën A, Valcke E (2011) Modelling of cation concentrations in the outflow of $NaNO_3$ percolation experiments through boom clay cores. Phys Chem Earth 36:1693–1699

Mayer KU, Frind EO, Blowes DW (2002) Multicomponent reactive transport modeling in variably saturated porous media using a generalized formulation for kinetically controlled reactions. Water Resour Res 38:1174. doi:10.1029/2001WR000862

Narasimhan TN, White AF, Tokunaga T (1986) Groundwater contamination from an inactive uranium mill tailings pile, 2. Application of a dynamic mixing model. Water Resour Res 22(13):1820–1834

Parkhurst DL, Appelo CAJ (1999) User's guide to PHREEQ C (version 2) – a computer program for speciation, batch-reaction, one-dimensional transport and inverse geochemical calculations, water-resources investigations. Report 99–4259, Denver, 312 pp

Parkhurst DL, Kipp KL, Engesgaard P, Charlton SC (2004) PHAST – a program for simulating ground-water flow, solute transport and multicomponent geochemical reactions. U.S. Geol Surv Tech Methods 6-A8, 154 pp

Parton WJ, Schimel DS, Cole CV, Ojima DS (1987) Analysis of factors controlling soil organic matter levels in Great Plains grasslands. Soil Sci Soc Am J 51:1173–1179

Ramos TB, Šimůnek J, Gonçalves MC, Martins JC, Prazeres A, Castanheira NL, Pereira LS (2011) Field evaluation of a multicomponent solute transport model in soils irrigated with saline waters. J Hydrol 407(1–4):129–144

Ramos TB, Šimůnek J, Gonçalves MC, Martins JC, Prazeres A, Pereira LS (2012) Two-dimensional modeling of water and nitrogen fate from sweet sorghum irrigated with fresh and blended saline waters. Agric Water Manage 111:87–104

Rasouli F, Pouya AK, Šimůnek J (2013) Modeling the effects of saline water use in wheat-cultivated lands using the UNSATCHEM model. Irrig Sci 31(5):1009–1024. doi:10.1007/s00271-012-0383-8

Reading LP, Baumgartl T, Bristow KL, Lockington DA (2012) Applying HYDRUS to flow in a sodic clay soil with solution composition–dependent hydraulic conductivity. Vadose Zone J 11 (2). doi:10.2136/vzj2011.0137

Regnier P, Dale AW, Pallud C, van Lith Y, Bonneville S, Hyacinthe C, Thullner M, Laverman AM, Van Cappellen P (2005) Incorporating geomicrobial processes in reactive transport models of subsurface environments. In: Nützmann G, Viotti P, Aagaard P (eds) Reactive transport in soil and groundwater. Springer, Berlin Heidelberg, pp 109–125

Rittmann BE, VanBriesen JM (1996) Microbiological processes in reactive modeling. In: Lichtner PC, Steefel CI, Oelkers EH (eds) Reactive transport in porous media, reviews in mineralogy, Chapter 7, vol 34. Mineralogical Society of America, Chantilly, VA, pp 311–334

Schoups G, Hopmans JW, Tanji KK (2006) Evaluation of model complexity and space–time resolution on the prediction of long-term soil salinity dynamics, western San Joaquin Valley, California. Hydrol Process 20:2647–2668

Seaman JC, Chang H, Goldberg S, Šimůnek J (2012) Reactive transport modeling. Vadose Zone J 11(2). doi:10.2136/vzj2012.0066, 7 pp

Šimůnek J (2005) Chapter 78: models of water flow and solute transport in the unsaturated zone. In: Anderson MG, McDonnell JJ (eds) Encyclopedia of hydrological sciences. Wiley, Chichester, pp 1171–1180

Šimůnek J, Suarez DL (1994) Two-dimensional transport model for variably saturated porous media with major ion chemistry. Water Resour Res 30(4):1115–1133

Šimůnek J, Suarez DL (1997) Sodic soil reclamation using multicomponent transport modeling. ASCE J Irrig Drain Eng 123(5):367–376

Šimůnek J, Valocchi AJ (2002) Geochemical transport. In: Dane JH, Topp GC (eds) Methods of soil analysis, part 4, physical methods, Chapter 6.9, 3rd edn. SSSA, Madison, pp 1511–1536

Šimůnek J, van Genuchten MT (2006) Contaminant transport in the unsaturated zone: theory and modeling, Chapter 22. In: Delleur J (ed) The handbook of groundwater engineering, 2nd edn. CRC Press, Boca Raton, pp 22.1–22.46

Šimůnek J, van Genuchten MTh, Šejna M, Toride N, Leij FJ (1999) The STANMOD computer software for evaluating solute transport in porous media using analytical solutions of convection-dispersion equation. Versions 1.0 and 2.0, IGWMC – TPS – 71. International Ground Water Modeling Center, Colorado School of Mines, Golden, 32 pp

Šimůnek J, van Genuchten MT, Sejna M (2008) Development and applications of the HYDRUS and STANMOD software packages, and related codes. Vadose Zone J 7(2):587–600. doi:10.2136/VZJ2007.0077

Šimůnek J, Jacques D, Šejna M, van Genuchten MTh (2012) The HP2 program for HYDRUS (2D/3D): a coupled code for simulating two-dimensional variably-saturated water flow, heat transport, and biogeochemistry in porous media, version 1.0, PC Progress, Prague, 76 pp

Šimůnek J, Jacques D, Langergraber G, Bradford SA, Šejna M, van Genuchten MTh (2013) Numerical modeling of contaminant transport with HYDRUS and its specialized modules, invited paper for the special issue "water management in changing environment", Mohan Kumar MS (ed) J Indian Inst Sci 93(2) 265–284. ISSN: 0970-4140 Coden-JIISAD

Skaggs TH, Shouse PJ, Poss JA (2006) Irrigation of forage crops with saline drainage waters: 2. Modeling drainage and root water uptake. Vadose Zone J 5:824–837

Steefel CI (2000) New directions in hydrogeochemical transport modeling: incorporating multiple kinetic and equilibrium pathways. In: Bentley LR, Sykes JF, Brebbia CA, Gray WG, Pinder GF (eds) Computational methods in water resources XIII. A.A. Balkema, Rotterdam, pp 331–338

Steefel CI (2009) CrunchFlow: software for modeling multicomponent reactive flow and transport, user's manual, 12 Oct 2009

Steefel CI, MacQuarrie KTB (1996) Approaches to modeling of reactive transport in porous media. In: Lichtner PC, Steefel CI, Oelkers EH (eds) Reactive transport in porous media. Reviews in mineralogy, Chapter 2, vol 34. Mineralogical Society of America, Chantilly, VA, pp 83–129

Steefel CI, DePaolo DJ, Lichtner PC (2005) Reactive transport modeling: an essential tool and a new research approach for the earth sciences. Earth Planet Sci Lett 240:539–558

Thaysen EM, Jacques D, Jessen S, Andersen CE, Laloy E, Ambus P, Postma D, Jakobsen I (2014a) Controls on carbon dioxide fluxes across the unsaturated zone of cropped and unplanted soil mesocosms. Biogeosciences (in review)

Thaysen EM, Jessen S, Postma D, Jakobsen R, Jacques D, Ambus P, Laloy E, Jakobsen I (2014b) Plant-mediated transfer of CO2 to aquifers as influenced by crushed concrete waste and lime amendments. Environ Sci Technol (in review)

Thullner M, Van Cappellen P, Regnier P (2005) Modeling the impact of microbial activity on redox dynamics in porous media. Geochim Cosmochim Acta 69:5005–5019

Toride N, Leij FJ, van Genuchten MT (1993) A comprehensive set of analytical solutions for nonequilibrium solute transport with first-order decay and zero-order production. Water Resour Res 29:2167–2182

United Nations Environment Programme (UNEP) (2002) Global mercury assessment. United Nations Environment Programme (UNEP), Geneva

VanBriesen J (1998) Modeling coupled biogeochemical processes in mixed waste systems, Ph.D. thesis, Civil Engineering. Northwestern University

Van der Lee J, De Windt L, Lagneau V, Goblet P (2003) Module-oriented modeling of reactive transport with HYTEC. Comput Geosci 29:265–275

van Genuchten MTh (1980) A closed-form equation for predicting the hydraulic conductivity of unsaturated soils. Soil Sci Soc Am J 44:892-898

van Genuchten MTh (1981) Analytical solutions for chemical transport with simultaneous adsorption, zero-order production and first-order decay. J Hydrol 49:213-233

van Genuchten MT, Šimůnek J, Leij FL, Toride N, Sejna M (2012) STANMOD: model use, calibration and validation, special issue standard/engineering procedures for model calibration and validation. Trans ASABE 5(4):1353–1366

van Genuchten MTh et al (2014) The use of numerical flow and transport models in environmental analyses. In: Teixeira WG, Ceddia MB, Ottoni MV, Donnagema GK (eds) Application of soil physics in environmental analyses: measuring, modelling and data integration. Springer, Cham

Viswanathan HS, Robinsons BA, Valocchi AJ, Triay IR (1998) A reactive transport model of neptunium migration from potential repository at Yucca Mountain. J Hydrol 209:251–280

Walsh SDC, Frane WLD, Mason HE, Carroll SA (2013) Permeability of wellbore-cement fractures following degradation by carbonated brine. Rock Mech Rock Eng 46:455–464

Walter AL, Frind EO, Blowes DW, Ptacek CJ, Molson JW (1994) Modeling of multicomponent reactive transport in groundwater 1. Model development and evaluation. Water Resour Res 30 (11):3137–3148

Xu T, Spycher N, Sonnenthal E, Zheng L, Pruess K (2012) TOUGHREACT user's guide: a simulation program for non-isothermal multiphase reactive geochemical transport in variably saturated geologic media, version 2.0. Report LBNL-DRAFT. Lawrence Berkeley National Laboratory, Berkeley

Yeh GT (1981) Analytical transient one-, two-, and three-dimensional simulation of waste transport in the aquifer system, ORNL-5602. Oak Ridge National Laboratory, Oak Ridge

Yeh G-T, Cheng H-P (1999) 3DHYDROGEOCHEM: a 3-dimensional model of density-dependent subsurface flow and thermal multispecies-multicomponent HYDROGEOCHEMical transport. EPA/600/R-98/159, 150 pp

Yeh GT, Tripathi VS (1991) A model for simulating transport of reactive multispecies components: model development and demonstration. Water Resour Res 27(12):3075–3094

Yuan F, Meixner T, Fenn ME, Šimůnek J (2011) Impact of transient soil water simulation on estimated nitrogen leaching and emission at high- and low-deposition forest sites in Southern California. J Geophys Res 116:G03040. doi:10.1029/2011JG001644, 15 pp

Zhang H, Nordin NA, Olsen MS (2013) Evaluating the effects of variable water chemistry on bacterial transport during infiltration. J Contam Hydrol 150:54–64

Zyvoloski GA, Robinson BA, Dash ZV, Trease LL (1997) Summary of the models and methods for the FEHM application – a finite element heat- and mass-transfer code. Los Alamos National Laboratory Rept. LA-13307-MS, Los Alamos